ISOTOPE PRODUCTION
IN LIGHT CHARGED PARTICLE INDUCED FISSION

BY
PEKKA P. JAUHO

Academic Dissertation
for the Degree of
Doctor of Philosophy

Jyväskylä, Finland
October 1994

ISOTOPE PRODUCTION
IN LIGHT CHARGED PARTICLE INDUCED FISSION

BY
PEKKA P. JAUHO

Academic Dissertation
for the Degree of
Doctor of Philosophy

To be presented, by permission of the
Faculty of Mathematics and Natural Sciences
of the University of Jyväskylä,
for public examination in Auditorium S-212 of the
University of Jyväskylä on October 28, 1994,
at 12 o'clock noon

Jyväskylä, Finland
October 1994

Table of contents

Parent correction in the yield of a daughter nucleus

Preface

This work has been carried out during 1990-94 at the Department of Physics in the University of Jyväskylä using the MC-20 cyclotron and the IGISOL facility. In addition, a series of experiments were carried out at the SARA-facility in Grenoble in connection with my three-months long stay in the Lyon University. After this, the last paper [Paper I] was prepared with the help of Professor Valery Rubchenya who paid critical attention to the quality of the experimental results.

Abstract

In this thesis the production of neutron-rich isotopes in the mass region A= 96 - 120 has been studied. Their yields have been extensively studied with the IGISOL isotope separator in the $^{238}U(p, f)$ reaction. Deuteron and alpha particle induced reactions have also been investigated. In connection with this work several new isotopes have been identified for the first time. Specifically, the decays of ^{110}Tc and ^{112}Tc are discussed. Cumulative mass distributions as well as independent isotopic distributions have been constructed. In the method used here the total kinetic energy of the fragments is integrated so that there is no energy selection and the yields are post-neutron emission values. A theoretical model described in one of the joined papers has been used to extract the preneutron emission yields. These results can be used for estimating the possibilities of production of new neutron-rich isotopes, e.g. at the IGISOL facility. In addition, they are necessary to help refining the existing fission models.

List of publications

The main results given in this thesis work have been reported in the following papers

I. Isotopic product distributions in the near symmetric mass region in proton induced fission of ^{238}U   https://doi.org/10.1103/PhysRevC.49.2036

P. P. Jauho, A. Jokinen, M. Leino, J. M. Parmonen, H. Penttilä, J. Äystö, K. Eskola, and V. A. Rubchenya, Phys. Rev. C 49, 2036 (1994).

II. Independent and cumulative yields of very neutron-rich nuclei in 20 MeV p- and 18 - 41 MeV d-induced fission of ^{238}U   https://doi.org/10.1103/PhysRevC.44.336

M. Leino, P. P. Jauho, J. Äystö, P. Decrock, P. Dendooven, K. Eskola, M. Huyse, A. Jokinen, J. M. Parmonen, H. Penttilä, G. Reusen, P. Taskinen, P. Van Duppen, and J. Wauters, Phys. Rev. C 44, 336 (1991).

III. Status report of the SARA IGISOL used in the study of the ^{238}U(α 40 MeV, f) reaction

A. Astier, R. Béraud, A. Bouldjedri, R. Duffait, A. Emsallem, M. Meyer, S. Morier, P. Pangaud, N. Redon, D. Barneoud, J. Blachot, J. Genevey, A. Gizon, R. Guglielmini, J. Inchaouh, G. Margotton, J. L. Vieux-Rochaz, J. Ärje, J. Äystö, P. Jauho, A. Jokinen, H. Penttilä, K. Eskola, M. E. Leino, and J. B. Marguette Nucl. Instrum. and Methods in Phys. Res. B70, 233 (1992). https://resolver.scholarsportal.info/resolve/0168583x/v70i1-4_c/233_srotsiot24mr.xml

IV. Collective structure of the neutron-rich nuclei, ^{110}Ru and ^{112}Ru

J. Äystö, P. P. Jauho, Z. Janas, A. Jokinen, J. M. Parmonen, H. Penttilä, P. Taskinen, R. Béraud, R. Duffait, A. Emsallem, J. Meyer, M. Meyer, N. Redon, M. E. Leino, K. Eskola, and P. Dendooven, Nucl. Phys. A515, 365 (1990). https://doi.org/10.1016/0375-9474(90)90590-I

V. LINGAT - linearly fitted gating: an accurate method for background-correction in two dimensional data sets

T. Lönnroth and P. P. Jauho, Nucl. Instrum. Methods in Phys. Res. A261, 549 (1987). https://doi.org/10.1016/0168-9002(87)90368-8

The main contribution of the author of this thesis is in the Papers I and II. The theoretical part in the Paper I is mainly written by V. A. Rubchenya. The author has participated in the experiments and the analysis for the Papers III and IV. The Paper V has been written based on the computer programming work done by the author.

1. Introduction

The main emphasis in this work has been put on the task how to produce medium heavy neutron-rich nuclei. There are in principle two methods: fission and fragmentation. The fragmentation [Ber92] needs a large accelerator providing high bombarding energies, which makes it difficult to perform elsewhere but in the biggest laboratories. This makes the charged particle induced fission reaction attractive as an alternative. It has been extensively applied in Finland, France, Belgium and Japan in connection with the IGISOL method since it is essential to have mass separation to select the isotope under study from the other fission products. Already much earlier the thermal neutron induced fission has been applied to mass separation together using a reactor for example in Studsvik, Sweden [Rud90, Fog92] or in the 1970's at the ILL-Grenoble (recoil separator Lohengrin and ion-source separator OSTIS [Lhe88]), or at the KFA-Jülich (gas filled recoil separator JOSEF [Lhe86]) or at Brookhaven (TRISTAN [Hil88]). The earlier knowledge in fission prior to the IGISOL studies or this work as an isotope production reaction is essentially from the spontaneous fission reaction and the thermal neutron induced fission reaction. The symmetric mass region had not been covered by these earlier studies of independent yields of isotopes [Wah88]. In the present work one has tried to find out how the charged particle induced fission can be applied to produce nuclei far from the valley of stability near masses close to half of that of the fissioning nuclei, i.e. A= 100-120.

The goal of this thesis work is to find new knowledge of isotopic distributions in charge particle induced fission and to present a frame work for studying these distributions in future experiments in the same area of the chart of nuclides. That is to provide a tool one can work with in order to design future experiments. In particle-induced fission the reaction occurs via fusion of the bombarding projectile with the target nucleus, leading to formation of the excited compound nucleus and subsequent fission. First, the excited compound system emits neutrons before the fission. Then the residual nucleus is split in two final nuclei, whose masses range

from about A= 80 up to A= 160 . The proton, deuteron and alfa induced fission of ^{238}U are among the simplest ways to make fission events.

The asymmetric peaks of the mass distribution are not of the same height and width. The position of the symmetric mass division can be estimated by integrating the whole mass distribution and taking an average value. A new theoretical model [Rubchenya, Paper I] has been applied to describe the isotopic distributions and mass distributions. In this work the mass region A= 96 - 120 is studied, especially the symmetric region when the mass A of the fragment is about a half of the compound nucleus mass. The experimental results show that it is possible to use this model to extrapolate the yields on the neutron-rich side of the isobaric distributions. In this model the calculations of the fission cross sections are carried out in the framework of statistical theory [Age87]. In this thesis, different fission modes are discussed briefly as a function of excitation energy. Mass distributions have been measured quite extensively in different fission reactions and in [Wah88] there is a model applied to describe charge distributions for neutron rich isotopes in different reactions, that is the thermal-neutron induced fission and spontaneous fission. In chapter 2 references are given also for charged-particle induced fission. The IGISOL method has been used to separate a mass chain from other fission products. The high energetic recoil fragments are slowed down in the target and are then thermalized in the high pressure helium stopping chamber. The charge exchange reactions in the helium atmosphere lower the charge state of the fission products to +1. The last step from +2 to +1 is a three body reaction with an electron and a neutral helium atom. The helium flow takes the fission products out of the chamber to the acceleration tube of the mass separator. Conventional nuclear spectroscopic methods have been used at the focal plane of the mass separator to measure the β-delayed γ-activities. In the experimental part of the thesis, chapter 4, a description of the method is given in some detail which reveals how the determination of

fission yields have been achieved. The results of this thesis are given in chapter 5 which is an extended description of the results mentioned in the papers included in this thesis.

2. Nuclear fission as a production method of neutron rich nuclei

2.1. General about fission

The overwhelming part of fission in the considered reactions is a fission of compound nucleus formed as a result of fusion. The compound nucleus is then de-excited by evaporating neutrons, γ-rays and fission which compete with each other. Also direct reactions can lead to fission; for example the (d, pf) reaction when one neutron is transferred into the system. In fission, a large variety of isotopes are produced with the same target projectile combination. The main general problem in fission fragment spectroscopy is that fragments have large kinetic energies which originate from the high energy release (due to the higher binding energy per nucleon at medium masses). In this chapter, fission mechanism is described in general terms with a special emphasis on fission as a production reaction of neutron rich nuclei.

The first theoretical understanding of nuclear fission was based on the liquid drop model[Van73]. In this picture, fission is described to result from the competition of surface forces against the repulsive force by the Coulomb field, causing the nucleus to stretch. The fissility parameter is expressed as $X = E_c(0)/(2E_s(0))$, where $E_c(0) = 0.71\ Z^2/A^{1/3}$ is the Coulomb energy and $E_s(0) = 17.8\ A^{2/3}$ is the surface energy of a spherical nucleus. Thus the parameter X goes like Z^2/A and it is a measure of how eager the nucleus is to undergo fission.

Nuclei with $Z^2/A > (Z^2/A)_{critical}$ are unstable against spontaneous fission according to the liquid drop model. Hence, fission occurs typically for heavy nuclei. Due to their large N/Z ratio the products are neutron rich. The lighter nuclei need high excitation energy to fission whereas in the uranium region the fission barrier height is only about 6 MeV. Numerical liquid drop calculations [Wag91] including multipoles up to $\lambda = 16$ lead to the fission barrier height relative to the ground states as $B_f = 0.83 \ E_s(0)(1-X)^3$.
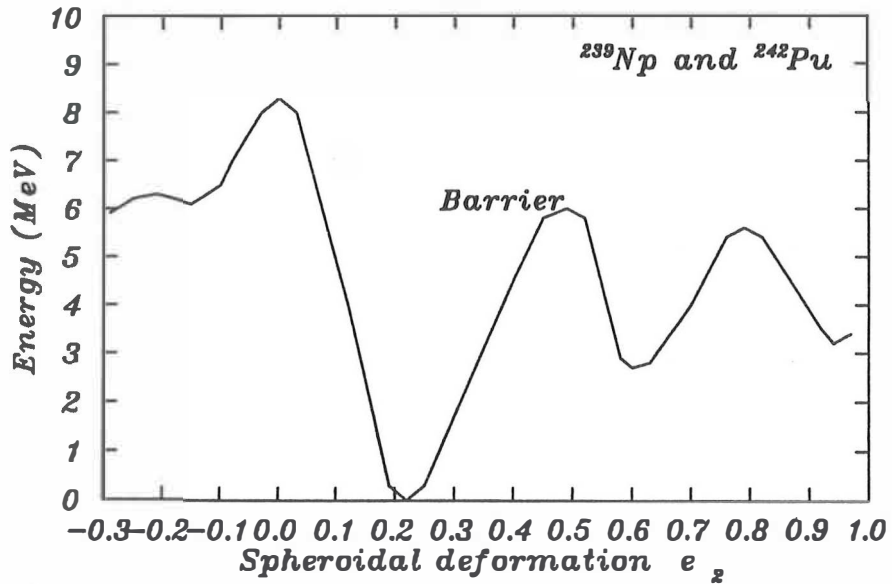
Fig. 1. Schematic representation of the two-humped fission barrier in ^{239}Np and ^{242}Pu [How80]. The figure illustrates the behaviour of the nuclear potential energy as a function of the spheroidal elongation coordinate ϵ_2.

The liquid drop model predicts spherical ground states for all stable nuclei, in contrast to observation, in particular for the actinides. In Fig. 1 there is a schematic representation of the two humped fission barrier as a function of the spheroidal deformation ϵ_2 [How80]. An

excitation energy higher than the fission barrier leads to prompt fission. The delayed fission already comes possible for lower excitation energy.

2.2. Modes of fission

In this section different fission modes as a function of the compound nucleus excitation energy are treated schematically.

2.2.1. Spontaneous fission

Spontaneous fission occurs for high $X = Z^2/A$ nuclei and is one form of natural radioactivity, because it proceeds from the ground state of the nucleus. Spontaneous fission [Van73, But92] is a rather rare decay mode, it occurs as a strong decay channel only for very heavy elements. There is only one spontaneously fissioning isotope $^{252}_{98}Cf_{154}$, which can be used as a source of

neutron-rich nuclei in practical spectroscopy. Its attractive features are: large N/Z and relatively small asymmetric component. As an example, the mass distribution of the products from the spontaneous fission of ^{252}Cf is shown in Fig.2. The total decay width is $\Gamma_{tot} = \Gamma_{fission} + \Gamma_\alpha$ corresponding to $T_{1/2} = 2.64$ y. The fission branching is 3 % [Led78]. The partial fission halflife depends on the fission barrier height and the barrier penetration probability. The data of Fig. 2 is from [Wah88]. Recently ^{248}Cm has been used in γ-spectroscopy experiments [Hot91].
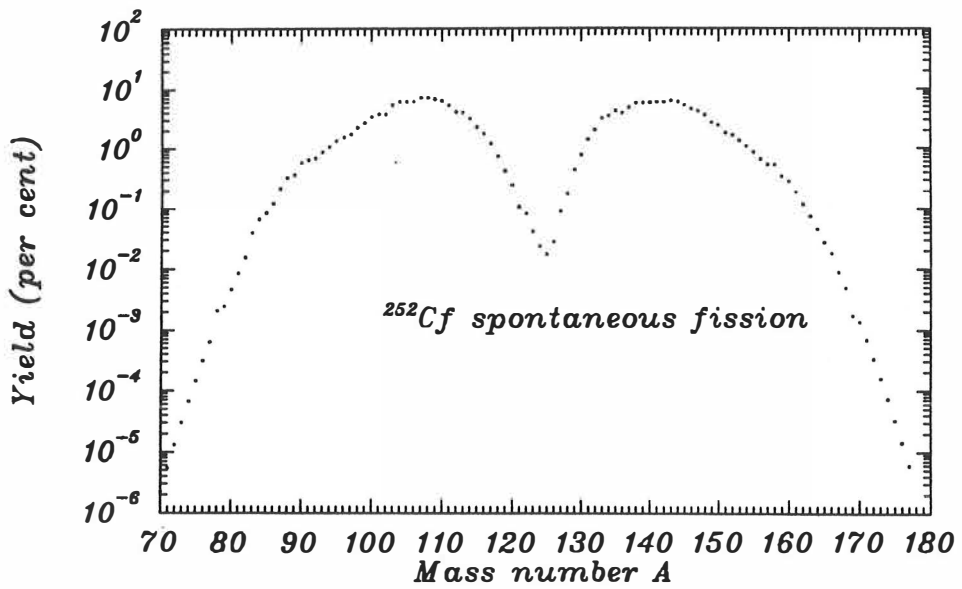
Fig. 2. Relative total mass distribution of fission products in spontaneous fission of ²⁵²Cf[Wah88].

2.2.2. Thermal neutron induced fission

Thermal neutron induced fission is another example of a rather low-energy fission mode. It may occur for compound nuclei with neutron binding energy B_n greater than the fission barrier B_f. Thus, the compound nucleus has more excitation energy than the spontaneously fissioning isotopes which have no excitation energy. The mass distribution for $n_{th} + {}^{235}U$ is shown in Fig.3. The excitation energy of the compound nucleus formed by the capture of a neutron by the target nucleus is trivially obtained from the ground state energies of the two partners and of the compound nucleus. For example in the thermal-neutron induced capture reaction ${}^{235}U + n$ the excitation energy of the compound system is 6.55 MeV. The reaction cross section for this resonance capture process is 583.5 barns, whereas for the capture reaction ${}^{238}U(n, \gamma)$ it is only 2.7 barns. As an example, the mass separated fission product beams at the mass separator Lohengrin [Hen94] has been used to determine the nuclear charge distribution for the thermal neutron-induced fission of ${}^{235}U$ for all light fission products in the region 80< A <107. The main references for the yields from the n_{th}-induced fission are [Wah88, Gäg78].
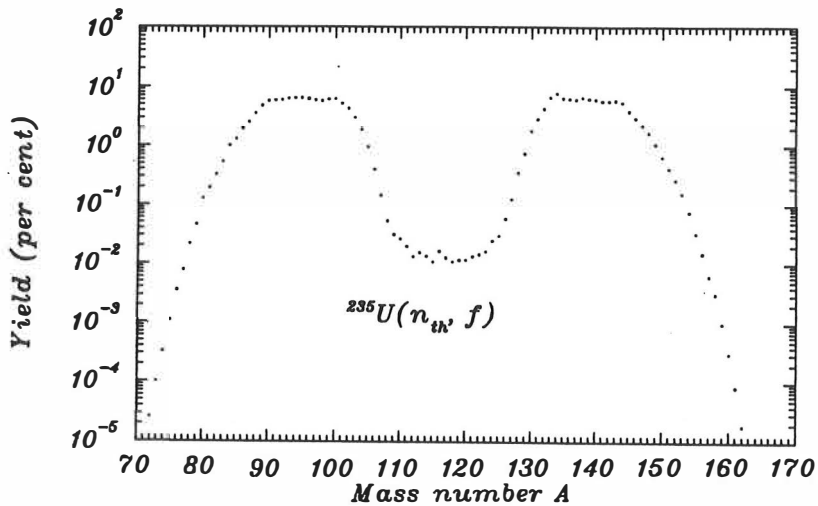
Fig. 3. Relative total mass distribution for the fission products in the reaction ${}^{235}U(n_{th}, f)$ [Wah88].

2.2.3. Charged particle induced fission

Charged particles feel a repulsive Coulomb force in the entrance channel of the fusion process. In a charged particle induced fission the compound nucleus excitation energy E_c vs. the fission barrier height B_f [Vio66, Sah80] has important consequences:

a) for elements before actinides there is a need for high E_c to overcome the high fission barrier B_f, which results in symmetric fission,

b) for actinides although the fission barrier is lower, high bombarding energy is needed to overcome the high Coulomb barrier in the entrance channel, which results in high excitation energy E_c and leads to a competition between symmetric and asymmetric fission.

For heavy ion fusion-fission reaction the probability for formation of neutron rich isotopes is unfavourable. When the compound nucleus excitation energy is much higher than the fission barrier no strong odd-even effects occur. In a heavy ion induced fission [Fab80, Kra76] there is a higher Coulomb repulsion and the compound nucleus gets more excitation energy than with light ions. In all cases there is a strong symmetric fission channel. Only "low" energy p- and d-induced fission possess also an asymmetric fission mode. In Fig. 4 the theoretical cross sections for the mass yields have been presented for the proton induced fission of ^{238}U at several bombarding energies. Alpha particles need already more than 40 MeV to overcome the Coulomb barrier, which leads to larger than 45 MeV excitation energy. Compare this with the fission barrier $B_f = 6$ MeV for the ^{238}U target. Light particles are used in this work. Heavy ions have been used at Daresbury [Gel88].
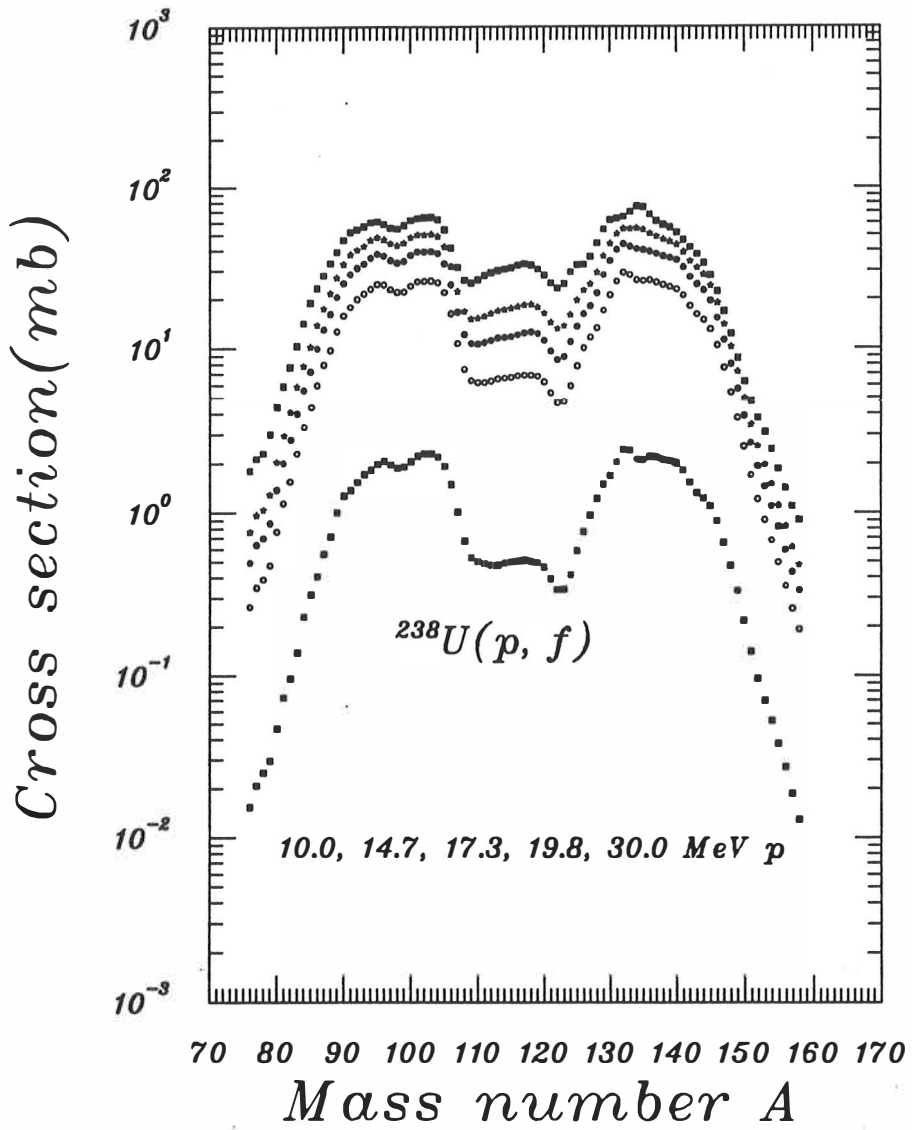
Fig. 4. Theoretical cross sections for the total mass yields of fission products in the proton induced fission of 238U with different bombarding energies [V. A. Rubchenya, Paper I]. Increasing proton energies increase the cross sections.

2.3. Mass and charge distributions

The compound nucleus fissions after no, one or several prompt neutron emissions, which means that multiple chance fission occurs mainly in a charged particle induced fission. The fragments form broad distributions in their atomic number (charge) and mass [Gäg78, Man78, Net77, Wah88]. The unchanged charge division is the simplest way to explain the average nuclear charge division. The mass distribution is more difficult to explain in a simple general way.

There is no exact theoretical model to describe the charge division between the two fragments. However the experimental charge distributions are often compared to the following postulates

a) Unchanged charge distribution (UCD), where the ratio of the proton and the neutron numbers is the same for the products as for the fissioning nucleus.

b) Potential energy minimisation, where the charge division correspond to the minimum of the potential energy at the scission point.

c) Equal charge displacement (ECD) in low energy fission, where the most probable charges of the products are equidistant from the line of betastability.

Usually the mass and charge distributions are given after the prompt neutron and γ-evaporation. The prompt neutron emission from the excited fragments occurs in $10^{-20\text{-}14}$ s after scission. The neutron multiplicity depends on the mass of the fissioning nucleus, the fragment mass and the excitation energy of the compound nucleus. Gamma- and conversion electron emission and X-ray emission follow in 10^{-14} -10^{-7} s after prompt scission. The shortest β-halflives are of the order of tens of ms, and extend up to "infinity". Therefore, β-decay does not play a role in the formation of independent primary fragment distributions.

In the case of p-induced fission, with proton-energy E_p, the sum of the total energy released in fission is the sum of the total kinetic energy TKE and of the fragment excitation energies $E_1^*(m_1)$, $E_2^*(m_2)$ [Van73]:

$$TKE(m_1, m_2) + E_1^*(m_1) + E_2^*(m_2) = Q_{eff} + S_p ,$$

where the effective Q-value can be written out in the form:

$$Q_{eff} = Q(m_c, m_1, m_2) + E_p - v(S_n + E_n),$$

where S_p (respectively S_n) is the separation energy of the projectile proton (ejectile neutron) from the compound system of a mass m_c and v is the number of evaporated neutrons.

(i) The mass distributions show yields increasing with E_p for symmetric scission. The peak yields in an asymmetric scission decrease and their locations shift slightly to lower values in the heavy fragment peak. This trend is well pronounced, if the mass distributions are considered as a function of the TKE, i.e. for different excitation energies of the composite system at the scission point. This observation reflects a competition of two different channels leading to fission, with their relative contributions varying with the compound nucleus excitation energy E_c. With increasing E_p, the channel that deals with the higher barrier [Wil76] or energy for neck rupture [Bro83] gains relatively high weight. This results in for ^{239}Np the super long channel leading to symmetric fission, high E_c and low TKE (excited fragments). It competes favorably with the standard channel [Bro83] for asymmetric fragmentation at higher TKE (cold fragments). Selecting the TKE isolates the two channels more effectively than the variation of E_c.

(ii) The average TKE as a function of mass split decreases with increasing compound nucleus excitation energy E_c in the region of the heavy fragment ($A_H = 132$), whereas for symmetric fragmentation this trend is reversed and persists for energies in E_p up to 25 MeV. It is so that in a more deformed system the distances are on the average larger and thus the electric repulsion smaller. As the TKE reflects the repulsion energy of the nascent fragments from the scission

point on, its decrease in the mass range $A_H = 132$ with increasing E_p indicates [Wil76] the relaxation of the reaction system with E_c towards higher deformation before separation of the fragments. In contrast, for the symmetric mass splits the system relaxes with increasing E_c towards smaller deformations because they are favored by the Strutinsky shell correction. In other words, an asymmetric system tends to become even more deformed when energy is added by E_p, this reduces TKE. A symmetric system tends to become less deformed due to shell effects, the more energy is added, this increases TKE.

(iii) The values for TKE corrected for fragment mass reduction by neutron emission continue to decrease with increasing E_p for $^{235,238}U$. The absolute values of TKE show no significant dependence on the target mass in this narrow mass region.

One useful approach to describe the probabilities of fission product formation is described in the Paper I [Kar91]. We take the fission cross section formula which describes the formation of the different fission chance nucleus A_c, Z_c at excitation energy E_c and hence the fission product A, Z by bombarding the target nucleus A_t, Z_t . The different fission chances refer to fission after no, one or several prompt neutrons.

$$\sigma_{pf}(A, Z, E_p) = \sum_{A_c, Z_c} \int dE_c \, Y_{post}(A, Z, A_c, Z_c) \frac{d\sigma_{pf}(A_t, Z_t, E_p, A_c, Z_c, E_c)}{dE_c},$$

Here one can take into account the calculated cross section of pre-neutron emission probabilities. The partial fission cross sections $d\sigma_{pf}/dE_c$ are calculated for E_p up to 30 MeV in the framework of the cascade evaporating statistical model including the pre-equilibrium neutron emission as in Ref. [Age87]. The independent fission product yields Y_{post} give the yield to obtain the nucleus A, Z from fission of the nucleus A_c, Z_c. They include neutron emission from the primary fragments. One should note that not only the first fission chance nucleus is referred with the letter c but all of them. Usually one calls only the first chance

nucleus as the compound nucleus. The other chances follow after prompt neutron evaporation of one or more neutrons. In each chance there is a possibility for fission.

3. Experimental method

3.1. IGISOL - technique

The principle of operation of the IGISOL (Ion Guide Isotope Separator On-Line)- technique is based on thermalization of primary recoil ions in helium and on their subsequent transfer by a helium flow through a differential pumping system into the acceleration stage of a mass separator[Tas89]. With this approach separation times of several orders of magnitude shorter than those typical of the ion-source-based systems are achieved. Energetic residual atoms produced in the nuclear reactions are in an ionized state, with their charge state proportional to the velocity. During thermalization these fast moving ions change their charge state continuously via charge-exchange processes with the atoms of the medium. In pure helium the slow -velocity recoils will keep their low charge states. Additional charge transfer and three body recombination processes in gas become however possible. Our experience with thermalized recoils produced in light-ions induced compound nuclear reactions shows that a large fraction of the recoils possesses a charge state +1 over a period of time long enough to be transported by a gas flow out of the thermalizing volume. Subsequently the thermalized ions are swept along with a 30-cm^3/s (standard temperature and pressure) flow through a 1.2-mm-diameter exit hole into an adjacent vacuum chamber. The positive ions are guided by an electric field over a distance of 10 mm through a 1.5-mm-diameter skimmer hole into the acceleration chamber of the mass separator, while most of the helium (neutral) is removed from the vacuum chamber by means of a high speed (2000 m^3/h) Roots blower. The mass separator coupled to the ion transportation system is of Scandinavian type equipped with a 55° analyzing magnet. The mass resolving power M/ΔM for the setup has been measured to be greater or equal to 400 (FWHM).

3.2. Stopping of fragments in the ion guide

The target in the ion guide setup serves both as a source of fission fragments and as an absorber. The fragments need to be slowed down to an energy which allow thermalization in helium. The ions loose their energy in the target both in inelastic and elastic collisions. Elastic collisions allow only small changes in the scattering angle. The fission fragments change their charge state all the way through the target and they have a charge state distribution when exiting the target. In helium all the charge states converge to +1 so the initial charge state distribution has no influence on the efficiency of the system. The TRIM program [Zie85] has been used to show that a 10 mg/cm^2 ^{238}U target thickness is effective as whole to produce fission products with 350 keV energy which can be thermalized in helium at a pressure of 10 kPa within an effective volume of about 10 cm^3, according to [Nor70] (Fig. 5 and 6). The TRIM program uses Monte Carlo simulation to follow the path of an ion in the target between different scattering events. Initially an isotropic angular distribution of fragments is assumed. The possible small deviation from isotropic distribution is not conserved in the target because of multiple scattering of the fission products. The TRIM program gives results in 2π geometry, i.e. the angular distribution of the exiting ions from the target and their energies. It also gives the number of backscattered ions. Several isotopes covering the mass region A= 96 - 120 were tested against energy selection by giving them an initial energy corresponding to the true fission kinetic energy and letting them fly through the target. The efficiency of the setup is most sensitive to the energy of the fission product but also the Z of the isotope should have some influence. No selectivity was found in the energy region corresponding to the mass region A = 96 - 120. The main interest in the yield experiment is based on the fact that the whole initial energy distribution is integrated in the IGISOL system so there is no energy selection.
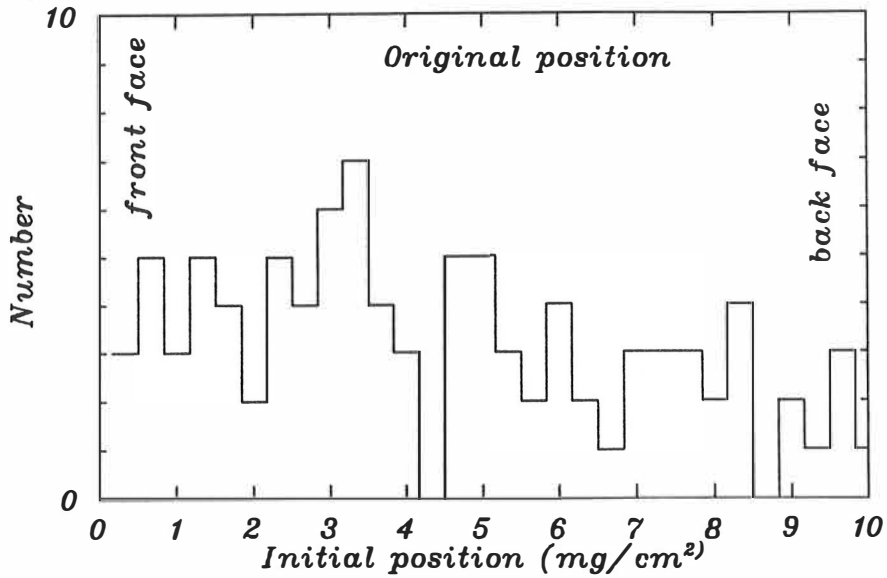
Fig. 5. The initial position of selected fission products inside the 10 mg/cm^2 natural U target thickness simulated with the TRIM program. The fragments from this distribution exit the target on the right side of the picture at the final energy of 350 keV or less. The number of calculated ions was 50000, which mostly have higher final exit energies (see Fig. 6).
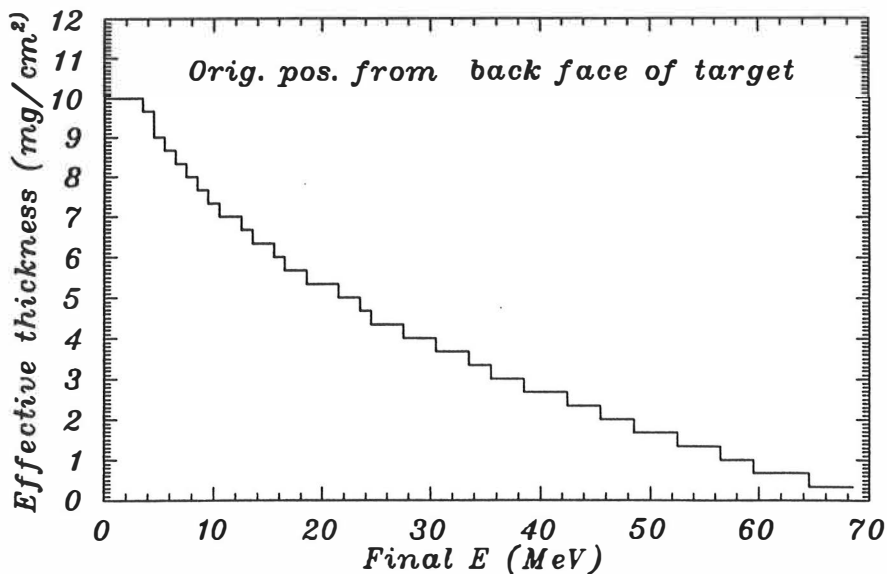
Fig. 6. The effective target thickness as a function of the final kinetic energy of the selected fission products. The thickness is taken from the back face of the target. The data is from the same TRIM calculation as in Fig. 5 with 50000 calculated ions. The initial kinetic energy of ^{96}Y ions is 101.4 MeV.

With the TRIM program one can calculate the number of ions which are slowed down to the 350 keV energy or less while starting from the initial kinetic energy. The all-in-all efficiency for thermalizing the fission product is about 10^{-3}. The efficiency of getting the thermalized ion from the helium chamber to the separator acceleration tube is about 40%. This number can be derived from the cross section comparison with a spectroscopic yield experiment [Kar91] done without mass separation (see Fig. 7). In that experiment the target was covered with absorber foils and the whole stack was then viewed by a γ-detector after the irradiation. The solid angle was thus 4π. In the IGISOL target system mainly single fission fragments are captured since the two fragments fly in opposite directions. A 2π geometry is assumed in the TRIM calculations i.e. the ions escaping from the target are studied within an angle of 90° relative to the beam

direction. However, the geometrical efficiency of IGISOL is 0.65 relative to 2π. Accordingly, the TRIM calculations need to be scaled with the latter ratio.

We used a 10.0 mg/cm^2 natural U target which is composed of ^{238}U to the amount of 99.2745%. The U target was covered with 0.2 mg/cm^2 Al foils on both sides to protect the target surfaces from oxidation. A 0.9 mg/cm^2 Ni foil separates the target chamber from the stopping volume of the IGISOL system [see Fig. 1 in Paper I]. In a first calculation, it is assumed that the Ni foil is placed on the target. We have observed no dependence on the nuclear charge Z nor the mass A of the fragments caused by the kinematics in the target in the studied mass region by using the TRIM computer program. It is assumed that initially the ions (A, Z) are distributed uniformly throughout the target, that they all have the same initial energy and that their initial direction has an isotropic distribution. By saving the initial angle parameters one can also verify that after the simulation the initial laboratory angle distribution has remained isotropic. We obtain the energy and angular distribution of the fission products leaving the target. The fraction of ions stopped in helium compared to the number of incident ions was calculated for some fission products at the region of interest.

A more refined analysis takes into account that the Ni foil is not on the target but separates the two IGISOL chambers from each other. First it was calculated as a function of the incident angle how much energy is left in the Ni foil by those ions that just escape the Ni foil with an average energy of 350 keV. The energy and angular distribution of the fission products leaving the target was then calculated without the Ni foil. From this distribution the number of ions with the energies which can leave the Ni foil with an energy of 350 keV were picked up. Also the fraction of ions escaping from the Ni foil with these input energies was calculated. The product of the given dependencies as a function of mass represents the refined TRIM correction to the mass distributions. Actually, no mass dependence of this kind was found by the simulation.

3.3. Setup and data acquisition

In the experimental setup γ-rays were detected with a 50 % Ge and a planar Ge X-ray detector all placed close to the focal point of the IGISOL system. In front of the big Ge detector a plastic ΔE-detector for the detection of β decay was used for gating the γ-rays. In the acquitsition setup we had 5 parameters: two γ-detector energy signals, ΔE energy signal and two time to digital converters TDC measuring number of events versus time with respect to absolute and cycle time, thus we measured β-γ-coincidences and γ-singles. The intensity of the proton beam in the yield experiments was stable to about 20 % only. Monitoring of the beam and the operation of the whole system was done using the detected activity as a yield monitor. A TDC was used to provide time of occurrence label on each β-coincident γ-event. One projection of the events was showing constantly the total time profile of the TDC, which revealed us if there was anything wrong in the separator or cyclotron. The observed cyclotron beam current after the target was written down regularly so the total TDC profile and the cyclotron beam current could be compared at certain times. In the final analysis the total TDC projections were integrated over the duration of the experiment and the effective acquisition times were determined which meant that the integrated yield was divided by the height of the profile in the position where the beam was known.

4. Analysis method

The large number of gamma-ray spectra resulted in a need to create special tabulation routines tailored for this analysis. First, the spectra have been analyzed using automatic peak search with the program SPANAL [Lhe91] which produces the peak areas and their statistical errors. Subsequently, the data have been analysed by a VAX computer using a set of fortran programs tailored for this purpose. The output lists of peak analysis have been scanned by a program which picks up the data for selected energies. Besides the file of peak energies two files were pre-edited. One is the acquisition data file including the acquisition times, beam intensities and the integrals of the TDC time profiles of $\gamma(\beta)$ yield and the other includes the branching ratios. The detection efficiency is given by a function of the γ-energy. The program YIELDS (see Fig. 6+) calculates the cumulative yields out of each listed γ-peak. It prints the effective acquisition time, the beam current, the β-efficiency, the element, the half-life, the peak energy, the γ-branching ratio, the γ-efficiency, the cumulative yield and the total statistical error for each yield.
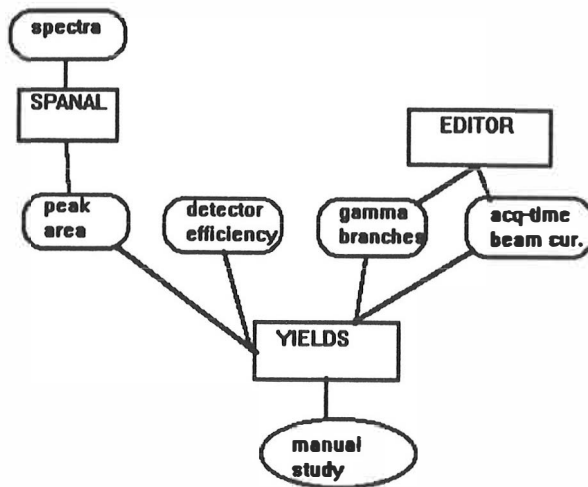
Fig. 6+. This is the arrangement to be sure of correct identification and yield analysis of γ-peaks.

The printouts of the program YIELDS form the basis for a later analysis of the cumulative and the independent yields. The independent yield distributions have been constructed out of the cumulative yield data by plotting successive A-distributions of Z and subtracting them from each other. The yields of the nuclei were corrected for the half-lives whenever necessary. However, the most elegant way to avoid the need for correction of the yield for halflife is to use long acquisition times after the beam was shut off so all the produced isotopes have a chance to be detected independently of their half-lives.

The coincident summing is less than about 4 % which has not been corrected but is included in the inaccuracy of the results. For some particular cases this has been taken into account because of the complexities of the decay schemes involved.

4.1. Evaluation of absolute γ-branching ratios

A major problem in finding out independent as well as cumulative yields is the determination of the intensity of the ground state branch in the β-decay of a nuclide. The method used to solve the problem varies from nuclide to nuclide. In some cases nuclear structure considerations exclude the existence of a strong ground state branch. But usually a careful study of the whole isobaric decay chain is necessary to determine the intensity of this branch.

The yield determination of a given isotope is based on the analysis of β-gated γ-ray radiation as well as of singles γ-ray spectra. The γ-branching ratios give a relation between the abundance of the β-decaying isotope and the number of specific γ-rays emitted. The number of useful γ-peaks is restricted by the fact that the γ-branching must be large enough to enable statistical accuracy. Note that the less abundant transitions are missed in the yield experiment because of relatively short acquisition times compared to actual spectroscopic studies. Very often the

lowest lying transitions are mixed so that both β-decaying isomeric state and the ground state populate the same level of which γ-decay is observed. However, in the yield analysis it is essential to find out the separate accurate yields of the ground state and isomeric state. In a favourable case the yield of one state, often the isomeric state, can be obtained through a pure transition. In the literature, in general, there are two branching ratios for the mixed transition, one for the isomeric state and one for the ground state decay. This information is however seldom available for the most exotic decays.

The determination of the β-branches to the γ-decaying states requires the full knowledge of the decay scheme. However, these β-intensities are often still only relative, because the β-branch leading to the ground state, called the ground state β-branch, is often unknown. The ground state β-branch can be deduced when the total β-intensity is measured in relation to the intensities of γ-transitions. The sum of the total intensities feeding the ground state plus the ground state β-branch must be 100 % of the decay. In this work two methods for solving this problem have been used [Jok91]. In the first one the intensity of the β-rays in the ΔE detector is compared with the γ-intensity. If there is no contamination, the integral of the singles β-energy-spectrum gives the total β-intensity and the β-gated γ-peaks give the required γ-intensities. The major difficulty in this method is to have a pure β-singles spectrum (free from contributions of isobaric decays) and the accurate knowledge of the β and γ efficiencies. Periodical acquisition mode in the experiment helps a little, because one can sometimes introduce a half-life-selection enhancement of the activity of interest.

The second method is based on the different time behaviour of the growth/decay of lines depending on mother/daughter contributions. In general, the yield relationship between the β-decaying parent and the daughter activity produced in fission, consists of a prompt component due to the direct daughter production in fission as well as of a time dependent component in the production rate arising from the feeding through the decay of parent. The time behaviour of the

yield is governed by the number of the β-decaying nuclei and their halflives. Since we usually know the γ-branches of the decay of the daughter nucleus, we can write a relation between the measured γ-yield of the daughter nucleus and the total β-yield of the parent nucleus. This requires that the experiment is performed in a periodical acquisition mode, beam on - beam off, and that the time dependent component in the γ-activity of the daughter nucleus arising from the parent nucleus can be resolved from the prompt daughter component. Formulas are shown in Appendix.

4.2. Constructing cumulative mass distributions

The major part of fission products are on the neutron-rich side of the stability line and hence they are β$^-$-active. The yields of isobars in a mass chain produced directly in fission (independent yield) are distributed according to the charge distribution as function of Z. The half-lives of the studied isotopes were all shorter than the acquisition times and the collection tape not moved so the activity of the isobar with the highest Z is cumulated. It is as big as the direct production yields of all the isobars in the same mass chain together. The activity of a nucleus is equal to the sum of the direct yield of it plus the parent yield. The advantage in this method is that the yields of all the isobars in the decay chain can be measured at the same time and there are no complex half-life corrections required.

For cumulative mass distribution one only needs the yield of the isobar with the highest observed Z. However, it should be checked that the selected isobar is well above the average $\overline{Z}$ of the mass chain. One can also consider doing a correction based on gaussian shape of the charge distribution if the Z of the chosen isobar is close to $\overline{Z}$. However, this kind of correction is always very uncertain and to be avoided if possible since it already relies on the estimate of $\overline{Z}$ and the variance σ_Z^2 of the charge distribution.

We have performed three studies of cumulative mass distributions. In all cases the IGISOL facility was used to separate the wanted mass chain from other fission products. One of them was done using the 20 MeV proton induced fission of ^{238}U, with four natural U targets in the IGISOL target chamber (see Fig. 1 in Paper II). The optimal cumulative yields in saturation of Tc, Ru, Rh, Pd, and Ag isotopes at the IGISOL separator are given in [Paper II]. Another study with a single target was aimed at receiving information on excitation functions since a single target allows more precise determination of the average excitation energy. A $\gamma(\beta)$ and low-energy singles γ-spectra were collected for about 1 or 2 hours at each mass position. The cyclotron and separator beams were continuous during these runs. This gave the saturated yields of isobars in a mass chain. Identifications of activities based on half-life information were only possible by monitoring the growth of certain peaks as a function of time. The duration of each run was decided considering the number of counts in the wanted γ-peaks during the production.

It is possible that the IGISOL method is somewhat sensitive to the elemental nature of separated isotopes due to differences in, for example, molecular formation and recombination rates. The Y, Zr, Nb, and Mo isotopes can be seen as oxides 16 mass units higher than their atomic mass. We have corrected this effect by adding the oxide yields to the atomic yields. The first thing to do is to compare the results with another experiment done using γ-spectroscopy without mass separation. This was done for the 17.3 MeV proton induced fission of ^{238}U since there was litterature data available[Kar91]. In Fig. 7 the measured IGISOL mass yields have been divided by the experimental fission product cross sections from Ref. [Kar91]. From this the IGISOL efficiency varies as a function of mass. Since the IGISOL efficiency should be only dependent on Z it would be good to integrate the isotopic mass distributions to have the total Z dependence of fission products measured with the IGISOL as raw data. However, it is hard to find litterature data to compare with. Thus in Fig. 7 there is an "artificial" mass dependence included since the total mass distribution is a function of Z also.
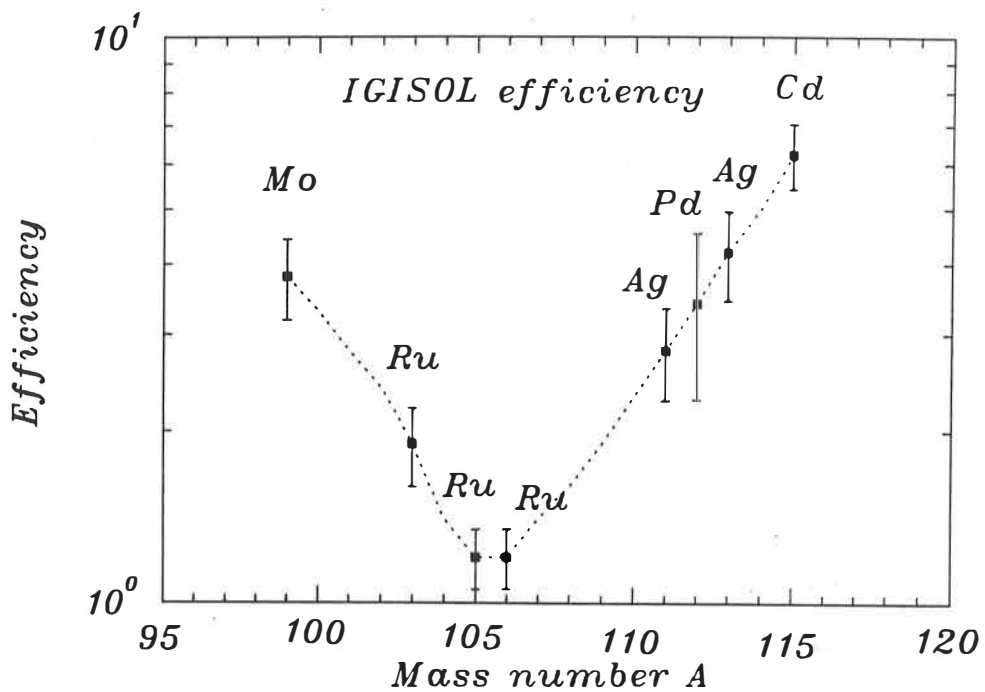
Fig. 7. The total mass yield ratios measured at IGISOL and Ref. [Kar91] for 17.3 MeV proton induced fission of ^{238}U. This gives the IGISOL efficiency relative to the γ-spectroscopic cross section study [Kar91] in arbitrary units.

5. Results

In this chapter major results of this thesis are reviewed. The results concerning the yields in the proton induced fission are given in the two papers included in this thesis. Also some results explained in the other papers of ours are discussed. When there are isomeric states for one nuclide, the yields of each isomer were summed.

5.1. Cumulative and independent isotopic yields

The mass region A= 108 -120 have been scanned to find out the yields of isotopes in the 20 MeV proton induced fission. The total thickness of uranium target material in the four target setup was 60 mg/cm^2 in the Jyväskylä experiments and 50 mg/cm^2 in the Louvain-La-Neuve experiments. The results should thus be considered averaged over the spread in proton and deuteron energy. The cumulative yields of Tc, Ru, Rh, Pd, and Ag isotopes in saturation are shown in Fig. 2 of Paper II. Also another study at IGISOL Jyväskylä has been done at the mass region A= 96 - 120. In order to get better description of the yields using a thinner target and accurately determined proton energy, the cumulative yield distributions were measured using a single 10.0 mg/cm^2 ^{238}U target using the proton energy of 19.8 MeV. The cumulative yields of Y, Zr, Nb, Mo, Tc, Ru, Rh, and Ag isotopes in saturation are shown in Table I of Paper I. The lower limits still visible in Fig. 2 of Paper II are removed due to the better knowledge of the ground-state branches in the later study of Paper I. Moreover, the error calculation has been included. Continuous proton beam was used and the collection of the activity at the focal point of the IGISOL separator was also continuous. The halflifes of the β-decaying isotopes are from a fraction of a second to some minutes, so their yields cumulate to the saturation condition among the isobars in a mass chain. The input data is presented in Table 1 [appendix], the nuclear halflife is marked with "c" if a halflife correction has been done. Usually there has been no need for halflife correction.

Using the SARA IGISOL facility and the reaction $^{238}U(\alpha, f)$ at E= 40 MeV, yields of very

neutron rich isotopes were studied in all mass chains from A= 96 to 122 (Fig. 11, [Paper III]).

The rather high excitation energy (35 MeV) of the compound nucleus leads to enhanced multiple

chance fission and thus to a rather complicated path to a final product. The overall mass yield

curve peaks at around A= 114-115, which means a strong prominence of symmetric fission

since more energy is brought into the compound nucleus than in proton induced fission.

Independent isotopic fission product distributions in the near symmetric mass region have been

measured for the first time. The independent isotopic mass distributions have been extracted for

Tc, Ru, and Rh (see Fig. 5. [Paper I]). The IGISOL efficiency correction has not been applied

to these distributions since they are at a constant Z value. The independent isotopic mass

distributions of Y, Zr, and Nb could not be determined because of inadequate information on

the absolute γ-branching ratios. One task was to compare the measured independent as well as

cumulative yields with the theoretical model (Fig. 5 [Paper I]). The theoretical cross sections

have been taken from Fig. 4. [Paper I] but they have been scaled with the factor 0.048

mb/(atoms/μC). As useful rule of thumb 1 mb corresponds to about 20 at/μC. The scaling is

based on the independent yield distribution of Tc since it shows the best shape of the three

experimental distributions available. A Gaussian form has been fitted to the experimental Tc

distribution with the total sum of 832 atoms/μC, the position $\overline{A}$ = 106.87(9) and the width

σ_A= 1.74(5). The total sum of the theoretical Tc distribution is 40.3 mb and thus one gets the

scaling factor which is independent of the small difference in the shapes of the experimental and

theoretical distributions. After the scaling one can see that the theoretical values are higher than

the experimental ones on the neutron-rich side of the distribution. The experimental point for

^{111}Tc is a lower limit because of the unknown ground-state β-branch. The parameters of the

theoretical Tc distribution are (Table II, Paper I): the position $\overline{A}$ =107.49, the width σ_A= 1.94

and the asymmetry parameter or the third moment of the distribution $b_A = 0.10$ which means that the isotopic distribution is not exactly of Gaussian shape but very close to that.

5.2. Isobaric yield distribution

One of the main results of this thesis is the charge dispersion at A= 112 and 114 (Fig. 5, [Paper II]), which yields experimental values for the most probable charge Z and the standard deviation σ_Z (Table I, [Paper II]). The experimental isobaric distributions show Gaussian form. In the case of A= 110 only the mean isobaric charge could be estimated due to a well established identification of only three nuclides: Tc, Ru, and Rh. In a very recent experiment at the upgraded IGISOL at the K-130 cyclotron ^{110}Mo decay has been observed with a yield of about 4 /s, i.e. about 1/35 of the ^{110}Tc yield[Lhe94].

At LLN, independent yields have been measured for A= 110, 112, and 114 using the d + ^{238}U reaction at bombarding energies 18, 25, and 41 MeV as indicated in Fig. 3 [Paper II]. In these experiments the target thickness was 50 mg/cm^2. At A= 112 no measurement was performed with E_d= 25 MeV. Prior to the present work, no experimental data on the decay of ^{114}Ru was available. The ^{114}Pd data are not shown because of the large uncertainty in the γ-branch of the 232 keV transition. Independent yields for A= 80 were also measured in a similar way. The mass yield at A= 80 seems to reach maximum value at 30 MeV bombarding energy (Fig. 4 Paper II). The dependence of $\overline{Z}$ on deuteron energy is weak. The excitation energy of the compound nucleus ^{240}Np is 33.0 MeV at 25 MeV deuteron energy. From this it can be estimated that fission of four nuclides $^{237-240}$Np contributes to the observed distribution at 25 MeV bombarding energy.

5.3. Yields of isomers

Isomeric states are very common among the studied nuclides. In cases where the isomeric state decays via competing β- and IT decays, the total β-branch is less than 100 % i.e. all the β-branches are normalized to the total number of β-decays (100 % - IT). The spin of an isomeric state is often high which means that it is not populated in β-decay but only directly in fission. The γ-decaying isomers are not observed in the γ(β) coincident spectra. Nevertheless, the feeding of γ-peaks are often mixed due to the isomeric and ground state β-population and they can be separated as explained in chapter 4. The parent yield has to be subtracted from the total ground state yield to deduce the ratios between the independent yields of the isomer and the ground state. The errors of the extracted isomeric yield ratios from our work are so large that no experimental values are shown in this thesis. Isomeric yield ratios of fission products in the system of 24 MeV proton-induced fission of ^{238}U have been studied in Ref. [Tan93].

5.4. New neutron rich nuclei ^{110,112}Tc

The decays of the new neutron rich nuclei ^{110}Tc and ^{112}Tc have been studied from the reaction ^{238}U(p, f), where E= 20 MeV. The production yields of these nuclei were typically 300 and 10 ions/μC. The layout of the experiment can be seen in Fig. 1 in Paper IV. The identification of these isotopes was based on earlier knowledge of the γ-decays and also on K X-ray coincidences. It is expected that the β-decay of the neutron rich nuclei in the studied mass region are mainly mediated by the $\nu g_{7/2} \rightarrow \pi g_{9/2}$ Gamow-Teller transition. However due to deformation, the ground states of odd-odd ^{110}Tc and ^{112}Tc have complex configurations and their β-strengths are spread over a large number of final states in the daughter Ru nuclei. We have measured β-decay, halflife $T_{1/2}$, end-point energies Q_{β}, γ-intensities I_{γ}, conversion electron intensities I(ce) and β-γ and γ-γ coincidences. In this way we have an idea of the

collective structure in ^{110}Ru and ^{112}Ru. Low-lying 2_2^+ indicates triaxiality. The static deformation of $^{108, 110, 112}$Ru have been investigated in microscopic lattice Hartree-Fock calculations. The obtained potential energy surfaces predict that these isotopes are triaxially deformed (β equals about 0.3) and do not favour prolate or oblate shapes. Lifetimes of the first excited 2_1^+ states in $^{106, 108, 110}$Ru have been very recently measured at the TRIGA-reactor in Mainz in order to determine the deformation [Sch96].

6. Discussion

In this chapter the reactions p, d, α + ^{238}U are discussed. The papers I , II, and III give cumulative isotopic yields as a function of mass number. The main difference in the three reactions is that the first one has been done using a thin target setup. The theoretical calculations reported in this thesis have been carried out by V. A. Rubchenya (Sec. V of Paper I and Ref. Kar91).

Cumulative mass yields near symmetric fission for 19.8 MeV p + ^{238}U are presented in Fig. 3 of the Paper I. The experimental mass yields are of high value at the symmetric mass region. The theoretical values have been scaled, comparing the integral of the measured independent isotopic yields of the Tc isotopes to the integral of the theoretical curve for Tc. One observes that the Rh isotopes agree well with the theory. These are the isotopes studied mostly with the IGISOL separator also in detailed spectroscopic experiments. The Ag isotopes agree also well up to A= 117. For higher masses the growing contribution of Cd isotopes should be included in the cumulative mass yields also. The Tc points are low, because the β-decay precursors Y, Zr, Nb, and Mo elements form oxides which move the ion beam off from the measured mass. The oxide yields have been added to the atomic yields of Nb but still the points are low compared to the theory.

The calculated parameters of the independent isotopic fission product distribution $\overline{A}$ and σ_A versus Z are presented for the reaction 19.8 MeV p + ^{238}U in Table II (Paper I) . One can note that the isotopic distributions are nearly symmetric since the third moments of the distributions are small. In Fig. 8 the average masses of the independent isotopic distributions are plotted as a function of the charge number. These can be compared to Fig. 4 [Paper I], where the calculated distributions are presented. Fig. 4 can also be used for predicting the cross sections of new isotopes. In Fig. 5 [Paper I] there is a comparison of the calculated and the measured

independent isotopic distributions for Tc, Ru, and Rh. The experimental values have been extracted from cumulative yields of Table I [Paper I]. Experimental Tc points agree fairly well with the theoretical points after the scales were adjusted. However, on the neutron-rich side they fall faster than the model estimates. Thus, it seems that the model overestimates the Tc yields on the neutron rich side of the distribution. The Rh yields agree well with theory as well for the shape as for the scale. However, the experimental yields for Ru are systematically smaller than the model prediction, especially the value for ^{108}Ru. This can be connected to some chemical effect in the IGISOL system which is not known. It is yet not clear, if this can be accounted for by a systematic error in absolute γ-branchings, which would have to be uncorrect in all measured Ru decays. Summarizing, regarding to isotopic distributions it seems that one should use the experimental distributions for extrapolation to new isotopic yields rather than the model.
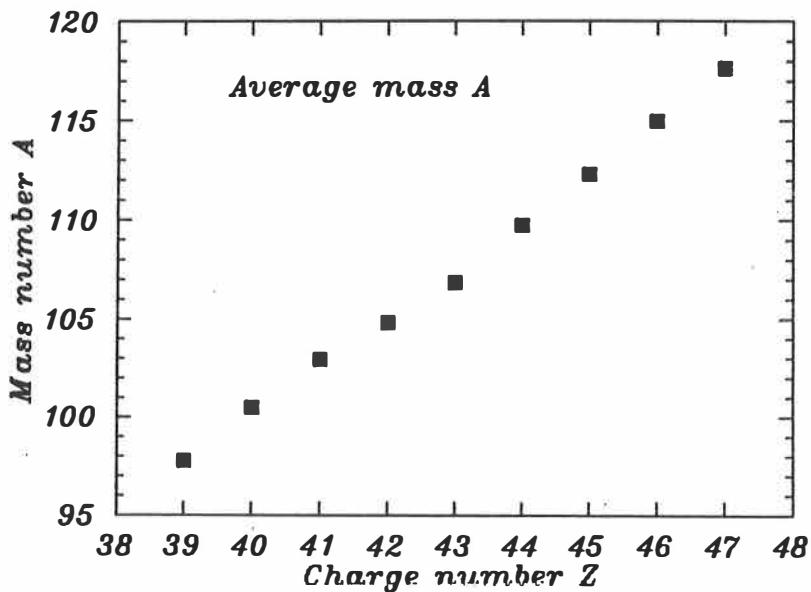
Fig. 8. The average masses of the theoretical isotopic distributions from Table II [Paper I]. σ_A is of the order of 1.7 - 1.9 mass units.

The cumulative yields obtained by 20 MeV p and the four target setup for Tc, Ru, Rh, Pd, and Ag isotopes in saturation are displayed in Fig. 2 (paper II). The dashed lines are drawn to guide the eye. The highest cumulative yields in Fig. 2 (paper II) give the mass distribution integrated over Z, which is seen in the region from A= 108 to 120.

Independent yields of A= 110, 112, and 114 are shown in Fig. 3 (paper II) for the d + ^{238}U reaction determined at three bombarding energies 18, 25, and 41 MeV. The 25 MeV yield versus atomic charge curve is quite similar to the 20 MeV p yields (Fig. 5 of the same paper). These reactions correspond to approximately the same excitation energy of the compound nucleus. The main result on relative independent yields of isotopes with A= 110, 112, and 114 for the 20 MeV p + ^{238}U reaction is illustrated in Fig. 9 and Table I of Paper II. The data for each isobaric chain was shifted in order to match the respective Z_{UCD} values. Experimental charge dispersion curves with widths from Table I (paper II) are drawn for A= 112 and 114. These charge distributions agree perfectly with the model of V. A. Rubchenya. Since the isobaric distributions are of Gaussian shape, the model can well be used to predict the yields for new isotopes at the symmetric mass region. The isobaric distributions are so narrow (σ_Z about 0.6) that only three experimental data points could be easily obtained in our experiments. The experiments for the isotopic mass distributions cannot be used to extract isobaric yield distributions because continuous cyclotron beam was used, which means that the data points for the higher Z values are very inaccurate since there would be a need for subtracting almost equal numbers from each other.
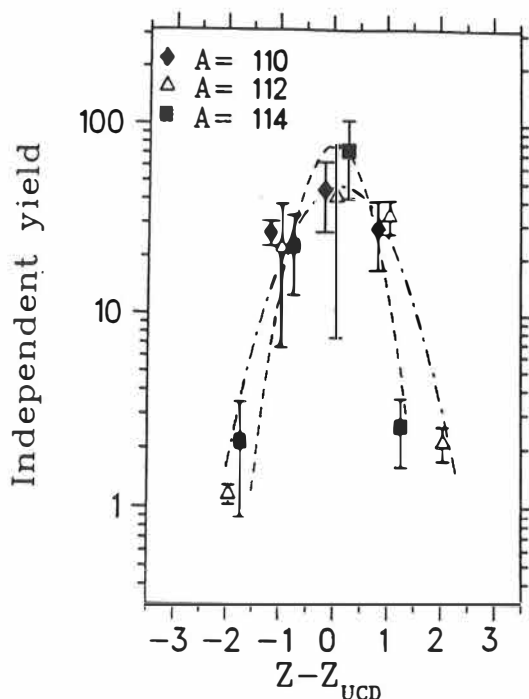
Fig. 9. Relative independent yields (in percent) of isotopes with A= 110, A= 112, and A= 114 from the 20 MeV p + ^{238}U reaction. The data for each isobaric chain was shifted using the respective Z$_{UCD}$ values [from Fig. 5, Paper II].

Fig. 11 in Paper III shows the yields in saturation for ^{238}U(α 40 MeV, f) reaction. This picture extends from the mass A= 96 up to 122 and can be compared with Fig. 2 in the paper II (20 MeV p, f). Comparison of the yields/μC for the reactions p + U, d + U, α + U shows that there are no large differences in the independent yields of neutron-rich isotopes around A= 110. In Table 2 (Appendix C) some predictions for cross sections of unknown isotopes according to the model of Paper I are presented.

7. Summary

Cumulative and independent yields have been measured for neutron-rich isotopes in the mass range A= 96 to 120, using fission of natural uranium induced by light charged particle beams. This work has been a cooperation between three laboratories, Jyväskylä, Louvain-La-Neuve and ISN-Grenoble/ IPN-Lyon, showing the excellent cooperation between universities on european level. The results are of crucial importance for the development of the knowledge of the fission process. In particular, the independent charge distributions are very rarely published material and are of high value, especially, in the mass region of symmetric fission. The validity of these results provides a reference material when planning new studies of the nuclear structure far from the stability or of decay properties, like half-life and delayed neutron emission probabilities, which are used as input parameters in astrophysical models. Thus it becomes possible to estimate production rates of new isotopes and whether the experiments are practicable.

References

[Age87]   V. A. Ageev, S. A. Egorov, V. Ya. Golovnya, E. A. Gromova,

           S. S. Kovalenko, A. F. Linev, Yu. A. Nemilov, A. V. Pozdnyakov,

           V. A. Rubchenya, Yu. A. Selitsky, A. M. Fridkin, and V. A. Yakovlev,

           Yad. Fiz. **46**, 1200 (1987) [Sov. J. Nucl. Phys. **46**, 700 (1987)].

[Äys87]   J. Äystö, P. Taskinen, M. Yoshii, J. Honkanen, P. Jauho, H. Penttilä, and

           C. N. Davids, Phys. Letters **201B**, 211 (1988).

[Äys88]   J. Äystö, C.N. Davids, J. Hattula, J.Honkanen, K. Honkanen, P. Jauho,

           R. Julin, S. Juutinen, J. Kumpulainen, T. Lönnroth, A. Pakkanen, A. Passoja,

           H. Penttilä, P. Taskinen, E. Verho, A. Virtanen, and M. Yoshii, Nucl. Phys.

           A480, 104 (1988).

[Äys90]   J. Äystö, P. Jauho, Z. Janas, A. Jokinen, J. Parmonen, H. Penttilä,

           P.Taskinen, R. Beraud,R. Duffait, A. Emsallem, J. Meyer, M. Meyer,

           N. Redon, M. Leino, K. Eskola, and P. Dendooven, Nucl. Phys. **A515**, 365

           (1990).

[Ber92]   M. Bernas, S. Czajkowski, J. L. Sida, Ph. Dessagne, Ch. Miehe, Ch. Pujol,

           P. Armbruster, R. Brissot, J. P. Bocquet, H. Faust, C. Kozhuharov,

           H. Geissel, E. Hanelt, G. Münzenberg, D. J. Vieira, G. Audi, and J. K. P. Lee

           Paper presented at 6th Int. Conf. on Nuclei Far From Stability & 9 th Int. Conf.

           on Atomic Masses and Fundamental Constants, Bernkastel-Kues, 1992, Inst.

           Phys. Conf. Ser. No 132: Section 5, page 557.

[Bla91b]   J. Blachot, Nuclear Data Sheets **64**, 1 (1991).

[Bla91c]   J. Blachot, Nuclear Data Sheets **62**, 709 (1991).

[Bro83]   U. Brosa and S. Grossmann, Z. Phys. A **310**, 177 (1983).

[Bro86]   E. Browne and R. B. Firestone, Table of Radioactive Isotopes, John Wiley &
            Sons (1986).

[But92]   K. Butler-Moore, S. Zhu, X. Zhao, J. H. Hamilton, A. V. Ramayya, Q. Lu,
            W. - C. Ma, L. K. Peker, J. Kormicki, J. K. Deng, P. Gore, D. Shi,
            E. F. Jones, H. Xie, W. B. Gao, J. D. Cole, R. Aryaeinejad, I. Y. Lee,
            N. R. Johnson, F. K. McGowan, C. E. Bemis, G. M. Ter-Akopian, and
            Yu Ts Oganessian, Paper presented at 6th Int. Conf. on Nuclei Far From
            Stability & 9 th Int. Conf. on Atomic Masses and Fundamental Constants,
            Bernkastel-Kues, 1992, Inst. Phys. Conf. Ser. No 132: Section 5, page 551

[Def91]   D. De Frenne and E. Jacobs, Nuclear Data Sheets **63**, 373 (1991).

[Den80]   H. O. Denschlag, Jahresbericht Mainz 1980.

[Fab80]   M. E. Faber, Z. Phys. **297**, 277 (1980).

[Fog87]   B. Fogelberg, E. Lund, Ye Zongyan, and B. Ekström, Contribution to 5th Int.
            Conf. Nuclei far from Stability, Rousseau Lake 1987.

[Fog90]   B. Fogelberg, Y. Zongyuan, B. Ekström, E. Lund, K. Aleklett, and L. Sihver, Z. Phys. **A337**, 251 (1990).

[Fog92]   B. Fogelberg, M. Hellström, D. Jerrestam, A. Kerek, H. Mach, L. O. Norlin, J. P. Omtvedt, and H. Prade, Paper presented at 6th Int. Conf. on Nuclei Far From Stability & 9 th Int. Conf. on Atomic Masses and Fundamental Constants, Bernkastel-Kues, 1992, Inst. Phys. Conf. Ser. No 132: Section 5, page 569.

[Gel88]   W. Gelletly, Y. Abdelrahman, A. A. Christi, J. L. Durell, J. Fitzgerald, C. J. Lister, J. H. McNeill, W. R. Phillips, and B. J. Varley, Proceedings of the International Workshop Bad Honnef, Fed. Rep. of Germany, April 24-28, page 101 (Springer-Verlag Berlin Heidelberg, 1988)

[Gäg78]   H. Gäggeler, H. R. von Gunten, Phys. Rev. C **17**, 172 (1978).

[Hen94]   R. Hentzschel, H. R. Faust, H. O. Denschlag, B. D. Wilkins, and J. Gindler, Nucl. Phys. **A571**, 427 (1994).

[Hil88]   J. C. Hill, F. K. Wohn, R. F. Petry, R. L. Gill, H. Mach, and M. Moszynski, Proceedings of the International Workshop Bad Honnef, Fed. Rep. of Germany, April 24-28, page 64 (Springer-Verlag Berlin Heidelberg, 1988).

[Hot91]   M. C. A. Hotchkis, J. L. Durell, J. B. Fitzgerald, A. S. Mowbray, W. R. Phillips, I. Ahmed, M. P. Carpenter, R. V. F. Janssens, T. L. Khoo,

E. F. Moore, L. R. Morss, Ph. Benet, and D. Ye, Nucl. Phys. A530, 111 (1991).

[How80]   W. M. Howard and P. Möller, At. Data and Nucl. Data Tables 25, 219 (1980).

[Jok91]   A. Jokinen, J. Äystö, P. Dendooven, K. Eskola, Z. Janas, P. Jauho, M. Leino, J. Parmonen, H. Penttilä, K. Rykaczewski, and P. Taskinen, Z. Phys. A 340, 21 (1991).

[Kar91]   E. Karttunen, M. Brenner, V.A. Rubchena, S.A. Egorov, V.B. Funschtein, V.A. Jakovlev, and Yu.A. Selitskiy, Nucl. Sci. And Engin. 109, 350 (1991).

[Kra76]   J. V. Kratz, J. O. Liljenzin, A. E. Norris, and G. T. Seaborg, Phys. Rev. C 13, 2347 (1976).

[Led78]   *Table of Isotopes*, 7th ed., edited by C. M. Lederer and V. S. Shirley (Wiley, New York, 1978).

[Lhe86]   G. Lhersonneau, D. Weiler, P. Kohl, H. Ohm, K. Sistemich, and R. A. Meyer, Z. Phys. A 323, 59 (1986).

[Lhe88]   G. Lhersonneau, K. - L. Kratz, H. Ohm, B. Pfeiffer, and K. Sistemich, Proceedings of the International Workshop Bad Honnef, Fed. Rep. of Germany, April 24-28, page 58 (Springer-Verlag Berlin Heidelberg, 1988).

[Lhe91]   By courtesy of G. Lhersonneau (Kernchemie Mainz).

[Lhe94]   G. Lhersonneau, A. Honkanen, M. Huhta, P. P. Jauho, A. Jokinen, M. Leino,
           M. Oinonen, E. Ollikainen, J. M. Parmonen, and J. Äystö, communication in
           the fission workshop at Chateau de Baume, May 1994, submitted to Z. Phys. A

[Mul86]   W. -W. Muller and D. Chmielewska, Nuclear Data Sheets **48**, 663 (1986).

[NDS]   Nuclear Data Sheets.

[Net77]   D. R. Nethaway, A. L. Prindle, William A. Myers, W. C. Fugua, and M. V.
           Kantelo, Phys. Rev. C **16**, 1907 (1977).

[Nor70]   L.C. Northcliffe and R.F. Schilling, Nucl. Data Tables **A7**, 233 (1970).

[Pen90]   H. Penttilä, J. Äystö, P. Jauho, A. Jokinen, J. Parmonen, P. Taskinen, K. Eskola, M.
           Leino, P. Dendooven, and C. Davids, Phys. Scr. **T32**, 38 (1990).

[Pen92]   H. Penttilä, thesis, University of Jyväskylä (1992).

[Rav92]   H. L. Ravn, B. Jonson, E. Kugler, A. Przewloka, D. J. Simon, K. Zimmer,
           and the ISOLDE Collaboration, Paper presented at 6th Int. Conf. on Nuclei Far
           From Stability & 9 th Int. Conf. on Atomic Masses and Fundamental
           Constants, Bernkastel-Kues, 1992, Inst. Phys. Conf. Ser. No 132: Section 8,
           page 919.

[Rud90]   G. Rudstam, Radiochim. Acta **49**, 155 (1990).

[Sah80]   C.- C. Sahm, H. Schulte, D. Vermeulen, J. Keller, H. -G. Clerc, K. -H.
             Schmidt, F. Hessberger, and G. Munzenberg
             Z. Phys. A **297**, 241 (1980).

[Sch96]   S. Schoedder, Thesis, University of Mainz, Institute for Nuclear Chemistry.

[Shi92]   N. Shinehara, S. Ichikawa, S. Baba, K. Tsukada, T. Ohtsuki, and J. Alstad,
             Radiochim. Acta **56**, 127 (1992).

[Tra72]   B.L. Tracy, J. Chaumont, R. Klapisch, J.M. Nitschke, A.M. Poskanzer, E. Roeckl,
             and C. Thibauldt, Phys. Rev. C **5**, 222 (1972).

[Tan93]   M. Tanikawa, H. Kudo, H. Sunaoshi, M. Wada, T. Shinozuka, and M.
             Fujioka, Z. Phys. A **347**, 53 (1993).

[Tas89]   P. Taskinen, H. Penttilä, J. Äystö, P. Dendooven, P. Jauho, A. Jokinen, and
             M. Yoshii, Nucl. Instrum. Methods **281**, 539 (1989).

[Van73]   R. Vandenbosch and J. R. Huizenga, *Nuclear Fission* (Academic, New York,
             1973).

[Vio66]   V. E. Viola, Jr., and B. D. Wilkins, Nucl. Phys. **82**, 65 (1966).

[Wag91]   C. Wagemans, *The Nuclear Fission Process* (CRC Press, Boca Raton,
             1991).

[Wah88]   A. C. Wahl, At. Data Nucl. Data Tables **39**, 1 (1988).

[Wil76]   B. D. Wilkins, E. D. Steinberg, and R. R. Chasman, Phys. Rev. C **14**, 1832 (1976).

[Zie85]   J. F. Ziegler, J. P. Biersack, and U. Littmark, *The Stopping and Ranges of Ions in Solids* (Pergamon, New York, 1985).

Appendix A

Parent correction in the yield of a daughter nucleus

Here we assume that there is no direct production of the daughter nuclei via fission and that the number of daughter nuclei N_2 and the number of parent nuclei N_1 are zero in the beginning of the periodical acquisition experiment. The growth-in-part goes in time from 0 to t_0 and the decay part starts from t_0. The number of the parent nuclei at time t is

$$N_1 = \frac{n_1}{\lambda_1} (1 - e^{-\lambda_1 t}),$$

where n_1 is the direct production rate of the parent nuclei in fission. After solving the linear differential equation

$$\frac{dN_2}{dt} = -\lambda_2 N_2 + \lambda_1 N_1$$

we have

$$N_2 = -\frac{\lambda_1 n_1}{(\lambda_1 - \lambda_2)\lambda_2} e^{-\lambda_2 t} + \frac{n_1}{\lambda_2} + \frac{n_1}{\lambda_1 - \lambda_2} e^{-\lambda_1 t} \ , \ 0 < t < t_0.$$

In saturation $N_2 = \frac{n_1}{\lambda_2}$. Suppose an initial condition $N_2(t=t_0) = \frac{n_1}{\lambda_2}$. Then at $t > t_0$

$$N_2 = \frac{n_1 \lambda_1}{(\lambda_1 - \lambda_2)\lambda_2} e^{-\lambda_2 (t-t_0)} - \frac{n_1}{\lambda_1 - \lambda_2} e^{-\lambda_1 (t-t_0)} .$$

One component is always negative. The negative term grows as a function of t towards zero. The positive term goes slower to zero.

Grand parent correction in the yield of a daughter nucleus

The number of daughter nuclei is now labeled N_3. Suppose $n_2 = n_3 = 0$ and that $N_1(t=0) = N_2(t=0) = N_3(t=0) = 0$. Now solving the linear equation
$$\frac{dN_3}{dt} = -\lambda_3 N_3 + \lambda_2 N_2 ,$$

leads to a solution

$$N_3 = -\frac{n_1\lambda_1\lambda_2}{\lambda_3(\lambda_1-\lambda_3)(\lambda_2-\lambda_3)}e^{-\lambda_3 t} + \frac{n_1}{\lambda_3}$$

$$-\frac{n_1\lambda_2}{(\lambda_1-\lambda_2)(\lambda_1-\lambda_3)}e^{-\lambda_1 t} + \frac{n_1\lambda_1}{(\lambda_1-\lambda_2)(\lambda_2-\lambda_3)}e^{-\lambda_2 t}, \ 0 < t < t_0.$$

In saturation $N_3 = \frac{n_1}{\lambda_3}$. On the decay period we take as an initial condition $N_3(t=t_0) = \frac{n_1}{\lambda_3}$. Now

$$N_3 = \frac{n_1\lambda_1\lambda_2}{\lambda_3(\lambda_1-\lambda_3)(\lambda_2-\lambda_3)}e^{-\lambda_3(t-t_0)}$$

$$+\frac{n_1\lambda_2}{(\lambda_1-\lambda_2)(\lambda_1-\lambda_3)}e^{-\lambda_1(t-t_0)} - \frac{n_1\lambda_1}{(\lambda_1-\lambda_2)(\lambda_2-\lambda_3)}e^{-\lambda_2(t-t_0)}, \ t > t0.$$

Appendix B

Table 1. Absolute γ-branching ratios of the studied isotopes. Letter "c" denotes the cases where halflife correction was done. The references are for the branching ratios.

	Nuclide	$T_{1/2}$	E_γ(keV)	I_γ(%)	Ref. [NDS]	Other ref.
A= 96	^{96}Y	c 9.6 s	146.7	35.1	**68**, 165	
A= 97	^{97}Sr	0.39 s	306.8	11.2	**46**, 604	
	^{97}Sr	0.42 s	954.4	24.0	"	
	^{97}Y	c 1.23 s	161.3	71.0	"	Bro86
	^{97}Y	c 3.50 s	296.6	1.2	"	
	^{97}Y	c 1.23 s	970.2	39.4	"	
	^{97}Y	c 3.50 s	1291.0	5.4	"	
A= 98	^{98}Sr	0.653 s	119.1	23.0	**67**, 693	Bro86
	^{98}Sr		444.4	8.0	"	Bro86
	^{98}Sr		480.3	2.5	"	
A= 99	^{99}Y	1.47 s	121.6	44.0	**48**, 663	
	^{99}Y	1.486 s	575.0	10.9	"	
	^{99}Y		613.9	5.3	"	
	^{99}Y		723.9	20.0	"	
	^{99}Y		1014.5	7.9	"	
	^{99}Zr		55.7	2.2	"	
	^{99}Zr		81.5	2.8	"	
	^{99}Zr		178.8	5.4	"	
	^{99}Zr		387.3	8.0	"	
	^{99}Zr	2.1 s	461.7	11.0	"	
	^{99}Zr	2.0 s	468.9	55.2	"	
	^{99}Zr		545.9	48.6	"	
	^{99}Zr		593.8	27.4	"	
	^{99}Zr		649.9	2.2	"	
	^{99}Nb	c 2.6 min	252.8	3.7	"	Mul86
	^{99}Nb	c 2.6 min	351.3	2.8	"	
A= 100	^{100}Y	c 0.74 s	212.3	78.0	**60**, 1	
	^{100}Zr	7.1 s	400.3	19.2	"	
	^{100}Zr		503.9	31.0	"	Den80
	^{100}Nb	c 2.99 s	600.2	65.0	"	
	^{100}Nb	c 2.99 s	768.7	8.8	"	
	^{100}Nb	c 2.99 s	927.9	7.1	"	
A= 101	^{101}Y	c 0.5 s	97.8	24.3	**63**, 305	

Appendix B

Table 1. Absolute γ-branching ratios of the studied isotopes. Letter "c" denotes the cases where halflife correction was done. The references are for the branching ratios.

	^{101}Y	c 0.5 s	232.3	9.1	"	
	^{101}Nb	7.1 s	157.4	12.8	"	
	^{101}Nb		275.9	40.0	"	
	^{101}Nb		440.8	8.8	"	
	^{101}Nb		466.0	7.2	"	
	^{101}Nb		479.5	7.6	"	
	^{101}Mo	c14.6 min	506.0	11.8	"	Bro86
	^{101}Mo	c14.6 min	590.8	22.5	"	
	^{101}Mo	c14.6 min	695.4	7.2	"	
	^{101}Mo	c14.6 min	1012.3	12.8	"	Bro86
	^{101}Tc	c14.2 min	306.6	88.0	"	Bro86
	^{101}Tc	c14.2 min	544.9	6.0	"	
A= 102	^{102}Nb		295.8	81.0	**63**, 373	
	^{102}Nb		447.0	20.0	"	Def91
	^{102}Nb		551.4	31.0	"	
	^{102}Nb		847.4	19.0	"	Def91
	^{102}Nb		1632.7	42.0	"	
	^{102}Mo	c11.3 min	147.8	3.8	"	Bro86
	^{102}Tc	c4.35 min	696.8	6.4	"	
A= 103	^{103}Zr		126.1	36.6	**68**, 311	
	^{103}Zr		150.5	27.0	**68**, 311	
	^{103}Zr		217.9	3.0	"	
	^{103}Nb	1.5 s	102.3	100	"	
	^{103}Nb		241.0	6.9	"	
	^{103}Nb		455.8	8.8	"	
	^{103}Nb		505.1	7.8	"	
	^{103}Nb		538.3	34.0	"	
	^{103}Nb		641.2	55.0	"	
	^{103}Nb		746.3	11.6	"	
	^{103}Nb		967.2	6.3	"	
	^{103}Mo	c67.5 s	45.5	2.5	"	
	^{103}Mo	c67.5 s	83.2	19.0	"	
	^{103}Mo	c67.5 s	423.9	13.1	"	
	^{103}Mo	c67.5 s	519.0	5.2	"	

Appendix B

Table 1. Absolute γ-branching ratios of the studied isotopes. Letter "c" denotes the cases where halflife correction was done. The references are for the branching ratios.

	^{103}Mo	c67.5 s	608.4	4.2	"	
	^{103}Mo	c67.5 s	687.8	1.4	"	
	^{103}Mo	c67.5 s	1040.2	4.3	"	
	^{103}Tc	c54.2 s	135.9	16.6	"	
	^{103}Tc	c54.2 s	174.0	2.8	"	
	^{103}Tc	c54.2 s	210.2	6.8	"	
	^{103}Tc	c54.2 s	388.5	2.2	"	
	^{103}Tc	c54.2 s	403.3	2.1	"	
	^{103}Tc	c54.2 s	501.2	2.4	"	
	^{103}Tc	c54.2 s	562.8	7.0	"	
A= 104	^{104}Nb		368.4	14.8	**41, 325**	
	^{104}Nb		477.4	13.9	"	
	^{104}Nb		619.9	67.2	"	
	^{104}Nb		771.3	11.1	"	
	^{104}Nb		812.0	15.2	"	
	^{104}Mo	c60.0 s	36.1	14.0	"	
	^{104}Mo	c60.0 s	45.8	8.0	"	
	^{104}Mo	c60.0 s	49.9	3.9	"	
	^{104}Mo	c60.0 s	54.8	8.6	"	
	^{104}Mo	c60.0 s	90.9	4.9	"	
	^{104}Mo	c60.0 s	375.8	4.7	"	Bla91b
	^{104}Mo	c60.0 s	420.9	2.6	"	Bla91b
	^{104}Tc	c18.4 min	357.8	89.0	"	Bla91b
	^{104}Tc	c18.4 min	530.4	15.6	"	Bla91b
	^{104}Tc	c18.4 min	535.0	14.7	"	Bla91b
	^{104}Tc	c18.4 min	792.4	2.5	"	
	^{104}Tc	c18.4 min	884.7	10.9	"	Bla91b
	^{104}Tc	c18.4 min	893.2	10.2	"	
	^{104}Tc	c18.4 min	1612.8	5.8	"	
A= 105	^{105}Nb	2.95 s	94.6	33.4	**68, 935**	
	^{105}Nb		246.0	26.3	"	
	^{105}Nb		309.7	10.8	"	
	^{105}Nb		514.4	34.0	"	
	^{105}Mo	c35.6 s	64.0	5.5	"	

Appendix B

Table 1. Absolute γ-branching ratios of the studied isotopes. Letter "c" denotes the cases where halflife correction was done. The references are for the branching ratios.

	^{105}Mo	c35.6 s	76.3	19.2	"	
	^{105}Mo	c35.6 s	85.2	25.0	"	
	^{105}Mo	c35.6 s	147.8	14.7	"	
	^{105}Mo	c35.6 s	197.8	3.5	"	
	^{105}Mo	c35.6 s	217.4	3.77	"	
	^{105}Mo	c35.6 s	249.9	9.25	"	
	^{105}Mo	c35.6 s	269.1	4.35	"	
	^{105}Tc	c7.63 min	107.8	9.6	"	Bro86
	^{105}Tc	c7.63 min	143.0	10.7	"	Bro86
	^{105}Ru	c 266.4 min	724.0	47.3	"	
A= 106	^{106}Nb	1.02 s	171.4	90.0	**53**, 73	Bro86
	^{106}Nb		350.3	35.1	"	Bro86
	^{106}Mo	c8.4 s	465.7	19.0	"	
	^{106}Mo	c8.4 s	618.8	6.1	"	
	^{106}Tc	c36.0 s	522.2	7.7	"	
	^{106}Tc	c36.0 s	720.5	6.9	"	
	^{106}Tc	c36.0 s	792.4	5.3	"	
A= 107	^{107}Tc	c0.35 min	102.4	21.0	**62**, 739	
	^{107}Tc	c0.35 min	106.3	7.6	"	Bla91c
	^{107}Tc	c0.35 min	176.8	9.2	"	Bla91c
	^{107}Ru	c3.75 min	193.9	9.9	"	
	^{107}Ru	c3.75 min	405.8	2.3	"	
	^{107}Ru	c3.75 min	462.5	3.7	"	
A= 108	^{108}Tc	5.0 s	242.0	87.0	**62**, 803	
	^{108}Tc		465.5	14.4	"	
	^{108}Tc		707.8	11.5	"	
	^{108}Ru	c4.55 min	164.9	28.0	"	Shi92
	^{108}Rh	c0.28 min	618.8	15.0	"	Bro86
A= 109	^{109}Tc		194.8	25.1	**64**, 913	Pen92
	^{109}Ru	c0.58 min	225.8	19.5	"	
	^{109}Ru	c0.58 min	819.9	4.4	"	
	^{109}Rh	c1.33 min	177.8	7.9	"	
	^{109}Rh	c1.33 min	249.0	6.0	"	
	^{109}Rh	c1.33 min	291.0	7.8	"	

Table 1. Absolute γ-branching ratios of the studied isotopes. Letter "c" denotes the cases where halflife correction was done. The references are for the branching ratios.

A=	isotope	halflife	energy	ratio	ref	source
	^{109}Rh	c1.33 min	326.5	56.0	"	
A= 110	^{110}Tc	0.92 s	240.4	85.0	**67**, 809	Ays90
	^{110}Ru	c0.27 min	112.0	25.0	"	Jok91
	^{110}Rh	c0.47 min	546.9	42.4	"	
	^{110}Rh	c0.47 min	687.6	25.8	"	
A= 111	^{111}Ru	2.12 s	303.5	15.8	**60**, 889	Pen92
	^{111}Rh	c0.18 min	194.8	1.09	"	Pen92
	^{111}Rh	c0.18 min	275.0	74.3	"	Pen92
A= 112	^{112}Tc	0.28 s	236.3	81.0	**57**, 443	Paper4
	^{112}Ru	1.75	82.1	7.0	"	Jok91
	^{112}Ru		244.3	7.0	"	Jok91
	^{112}Ru		326.7	22.0	"	Jok91
	^{112}Rh	c0.11 min	534.2	28.0	"	
	^{112}Rh	c0.11 min	559.9	49.0	"	Äys88
A= 113	^{113}Ru	0.80 s	262.9	60.0	**59**, 729	Pen92
	^{113}Rh	2.80 s	189.3	21.3	"	Pen92
	^{113}Rh		348.8	45.2	"	Pen92
	^{113}Pd	c1.5 min	95.8	4.8	"	
	^{113}Pd	c1.5 min	643.7	6.0	"	Fog87
	^{113}Pd	c1.5 min	739.7	4.8	"	Fog87
	^{113}Ag	70.0 s	316.0	10.0	"	
A= 114	^{114}Rh		316.9	22.3	**60**, 139	
	^{114}Rh	1.85 s	519.8	48.0	"	Äys88
	^{114}Rh		678.9	26.4	"	
	^{114}Pd	c2.4 min	231.8	2.5	"	
	^{114}Ag		558.0	17.6	"	Fog90
A= 115	^{115}Rh	0.99 s	295.5	17.0	**67**, 1	Äys87
	^{115}Ag		228.8	18.0	"	
A= 116	^{116}Ag		513.3	76.0	"	
	^{116}Ag	8.2 s	1029.3	26.5	**59**, 333	
A= 117	^{117}Ag		135.0	23.0	**66**, 451	
	^{117}Ag	72.4 s	337.7	10.3	"	
A= 118	^{118}Ag		487.4	81.0	**51**, 329	
	^{118}Ag		770.9	11.3	"	

Appendix B

Table 1. Absolute γ-branching ratios of the studied isotopes. Letter "c" denotes the cases where halflife correction was done. The references are for the branching ratios.

A= 119	^{119}Ag	2.1 s	626.4	15.6	67, 327

Appendix C

Table 2. A list of theoretical cross sections in the reaction ^{238}U(p, f), E_p= 20 MeV [Paper I], for the unknown isotopes which are in practical production limits of the IGISOL separator connected to the K-130 cyclotron. The new isotope ^{110}Mo has been produced with a rate 4 /s with the new IGISOL system with a 2 μA p beam. The theoretical cross section is σ= 0.580 mb.

	Z	A	σ[mb]	A	σ[mb]
Y	39	103	0.41	104	0.094
Zr	40	106	0.44	107	0.070
Nb	41	108	0.47	109	0.053
Mo	42	111	0.11	112	0.012
Tc	43	113	0.12	114	0.019
Ru	44	115	0.23	116	0.022
Rh	45	118	0.060	119	0.020
Pd	46	121	0.13	122	0.013